Observing solute transport in the capillary fringe using image analysis and electrical resistivity tomography in laboratory experiments

Persson, Magnus; Dahlin, Torleif; Günther, Thomas

Published in:
Vadose Zone Journal

DOI:
10.2136/vzj2014.07.0085

2015

Special Section: Dynamic Processes in Capillary Fringes

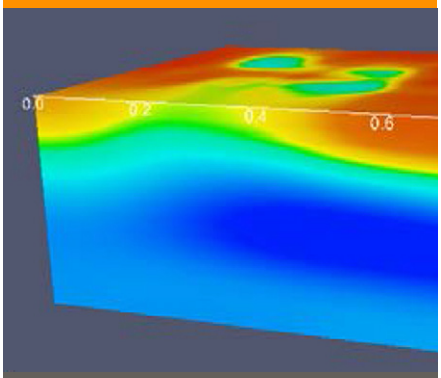

Laboratory experiments were carried out in a sand tank with saturated and unsaturated zones and a capillary fringe in between. Dye infiltration was monitored with image analysis and resistivity measurements. The results showed that solutes are transported horizontally in the capillary fringe with the same velocity as in the groundwater.

Observing Solute Transport in the Capillary Fringe Using Image Analysis and Electrical Resistivity Tomography in Laboratory Experiments

Magnus Persson,* Torleif Dahlin, and Thomas Günther

Five laboratory experiments were conducted to study solute transport in the capillary fringe in a sand-filled glass tank containing an artificial groundwater zone, an unsaturated zone, and a capillary fringe in between. Dye-stained water, applied at the soil surface, moved downward through the unsaturated zone and then horizontally in the capillary fringe. The horizontal velocity of the dye plume front was calculated using optical image analysis and electrical resistivity tomography (ERT) measurements. Both methods gave similar velocities if an appropriate value of the threshold ratio describing the dye front was used. The hydraulic model HYDRUS-2D was used to simulate dye movement in the glass tank. After calibrating the dispersivity value in the hydraulic model, the horizontal velocity was found to be in the range −10 to 17% compared with the values measured using image analysis and −12 to 24% compared with the values measured by ERT; the differences could probably be attributed to uncertainties in the hydraulic parameters and soil heterogeneities. Both experimental and numerical results showed that the horizontal velocity of the capillary fringe is more or less identical to the one in the saturated zone. Thus, from a water transport perspective, the results suggest that the capillary fringe should be treated as a part of the saturated zone in hydrologic modeling.

Abbreviations: CF, capillary fringe; ERT, electrical resistivity tomography.

The unsaturated zone, situated between the groundwater table and the soil surface, plays an important role in all ecosystems and constitutes the base on which the food chain is built. Another important aspect of the unsaturated zone concerns the recharge of groundwater. Groundwater constitutes an important water supply component for several purposes, such as domestic, industrial, and agricultural use, and is often considered as a clean water resource. However, polluting solutes from the soil surface can be transported down through the soil, contaminating the groundwater.

The capillary fringe (CF) includes the saturated and near-saturated layer directly above the groundwater table (e.g., Bear, 1972). In more general terms, the CF is the transition zone between the mainly vertical flow in the unsaturated zone and the mainly horizontal flow in the saturated zone. In coarse materials the CF is only a few centimeters thick, whereas it can be several meters thick in fine-textured materials. The lower boundary of the CF is the water table, i.e., the isoline at which the matrix potential is exactly 0. Zones with negative matrix potential that are fully saturated constitute the lower part of the CF. There is no generally accepted definition of the upper boundary of the CF. Instead, there are several different definitions, e.g., the highest level above the groundwater table that supports a continuous water column in saturated pores (e.g., Abdul and Gillham, 1984), the level above the water table equal to the air-entry value, i.e., the minimum suction that

M. Persson, Dep. of Water Resources Engineering, Lund Univ., Box 118, 211 00 Lund, Sweden; T. Dahlin, Engineering Geology, Lund Univ., Box 118, 211 00 Lund, Sweden; and T. Günther, Leibniz Institute for Applied Geophysics (LIAG), Stilleweg 2, 30655 Hannover, Germany. *Corresponding author (magnus.persson@tvrl.lth.se).

Vadose Zone J.
doi:10.2136/vzj2014.07.0085
Received 11 July 2014.
Accepted 13 Jan. 2015.

must be applied to a saturated soil to remove water from the largest pores (e.g., Gillham, 1984), or the point where the water content reaches a predefined water content lower than saturation (Ronen et al., 1997). Air entrapment is possible below as well as above the water table. This is especially true for fluctuating water tables and heterogeneous soil materials. The simultaneous presence of large quantities of both water and air at the same elevation makes the CF a suitable environment for biodegradation processes and important chemical reactions (Sinke et al., 1998; Abit et al., 2012).

Studies specifically focusing on the CF are less frequent than studies of water and solute transport in both unsaturated and saturated zones. The reason for this is probably twofold. First, detailed measurements, especially under field conditions, are very difficult to obtain in the CF, and second, processes in the CF are normally considered to be of minor importance. The lack of experimental data has prevented full understanding of the processes taking place in the CF. Berkowitz et al. (2004) and Dunn et al. (2005), among others, have highlighted the need for further studies of the CF.

Several laboratory experiments specifically focusing on the processes in the CF have been presented. Lehmann et al. (1998) studied the water flow through the CF in a small soil column with fluctuating saturation at the lower column end. They found that hysteresis had significant effects on the water content dynamics in the column. Silliman et al. (2002) used a transparent flow cell with both saturated and unsaturated sand. Using dye-stained water injected at several points, they showed that exchange of water below and above the water table occurs, with both upward and downward flow as well as a significant horizontal flow component. Similar setups have been used by other researchers. Klenk and Grathwohl (2002) studied the mass transfer of trichloroethene across the CF. They found a larger dispersivity in the CF than in the groundwater, a result of increased tortuosity due to entrapped air in the CF. Cho and de Rooij (2002) presented a study on the dissipation of preferential flow fingers conducted in a small flow cell. Much effort has been put recently into research on the formation of fingers and other types of preferential flow, but this is one of very few studies that is researching what happens to fingers reaching the CF. From a large-scale solute transport perspective, this should be important. It is our belief that studies of solute transport heterogeneity in the unsaturated zone are meaningless from a groundwater perspective if the processes in the CF are not considered.

Field studies specifically devoted to investigations of processes within the CF are scarce. Ronen et al. (1997) measured the gravimetric water content in the CF using soil samples collected with augers. Even though their measurements were performed in relatively homogeneous sand, substantial variability of the CF height was found. They also found that the CF was discontinuous, leading to the fact that horizontal flow in the CF was only possible above a critical height of the water table. In a later study (Ronen et al., 2000), they showed that the CF retained this feature even after a rainy season with groundwater recharge. They also found significant amounts of air at depths exceeding 1 m below the water table. Freitas and Barker (2011, 2013) studied the release of dissolved gasoline compounds and found that horizontal transport of both ethanol and hydrocarbon compounds in the CF was significant. Thus, when monitoring pollutant spreading, it is important to measure concentrations not only in the saturated zone to accurately define the pollutant plume.

As mentioned above, several studies have proved a substantial horizontal flow component in the CF. In most of these studies, the horizontal movement was observed and described qualitatively, e.g., Wyckoff et al. (1932), Henry and Smith (2002), and Silliman et al. (2002). Very few studies tried to quantify the horizontal flow and its dependence on, e.g., the hydraulic gradient. One example of an attempt to relate the horizontal flow in the CF to that in the saturated zone is the study of Abit et al. (2012). They studied solute movement in the CF in a laboratory flow cell and showed that the vertical extension of the solute plume can be explained by the fraction of the applied pulse to the total horizontal flow (return flow + flow of the applied pulse). They found a 1:1 relationship, i.e., if the applied pulse was 50% of the total flow, the solute plume occupied 50% of the total cross-section (including the saturated zone and the CF). If this relationship is true, it means that the horizontal velocity is exactly the same in both the saturated zone and the CF.

The CF is a region where processes are different from those in the saturated and unsaturated zones. According to recent research, the CF should not be treated as a simple boundary between the unsaturated and saturated zones. In modeling transport in the unsaturated zone, this boundary is often treated as either a constant-head or a constant-flux boundary. Instead, the combination of the CF with the regions immediately above and below is a unique interface that deserves focused studies. The fact that measurements specifically investigating these processes are difficult to make has led to understanding of this region being rather poor. Thus, there is a great need for further laboratory and field experiments using appropriate instrumentation.

The objectives of the present study were (i) to measure the horizontal velocity in the CF and investigate how it varies according to the groundwater gradient and infiltration rate, and (ii) to investigate if a hydraulic model can accurately describe the flow patterns in the CF. To this end, measurements were made in a laboratory glass tank using both optical image analysis and electrical resistivity tomography (ERT).

Materials and Methods

Experimental Setup

Laboratory solute transport experiments were conducted in a glass tank that was 1.50 m long, 0.49 m high, and 0.48 m wide.

The tank consisted of a saturated–unsaturated domain with an inner width of 1.22 m. On each side of this domain, two smaller reservoirs, each with an inner width of 0.1 m, were situated. A schematic sketch of the tank can be seen in Fig. 1, and a photograph is shown in Fig. 2. The main domain was filled to a height of 0.3 m with sand with a grain size of 0.3 to 0.7 mm to a bulk density of 1.5 g cm^{-3}. The reservoirs were used to adjust the gradient of the saturated zone. A pump with adjustable flow circulated water from the right reservoir to the left. To assure that the water levels in the reservoirs remained constant throughout the experiments even after injection of the tracer, a second pump was connected to a water level switch in the right reservoir. The water level in the right reservoir was set to 0.08 m for all experiments. The water level in the left reservoir varied between 0.09 and 0.12 m, depending on the desired gradient (see Table 1). In the tank, a three-layer regime was established: a saturated zone, the CF with a height of 0.13 m, and an unsaturated zone of approximately 0.08 to 0.1 m on top.

The dye tracer Brilliant Blue FCF was used to visualize water and solute transport across the CF. This dye has been used in several previous studies as it has proved to have good visibility, low toxicity, and weak adsorption on soils (e.g., Flury and Flühler, 1994; Persson, 2005b). The dye was infiltrated at a distance of 0.4 m from the left reservoir across the whole width of the tank. The tracer application system consisted of four separate pipes, each with a length of 0.1 m. Holes with a diameter of 0.0005 m were drilled at a spacing of 0.025 m along the underside of the pipes. Both ends of each pipe were connected with plastic tubes to a Masterflex L/S pump (Cole Parmer) with an adjustable flow rate. More details of the setup can be found in Pojmark et al. (2011).

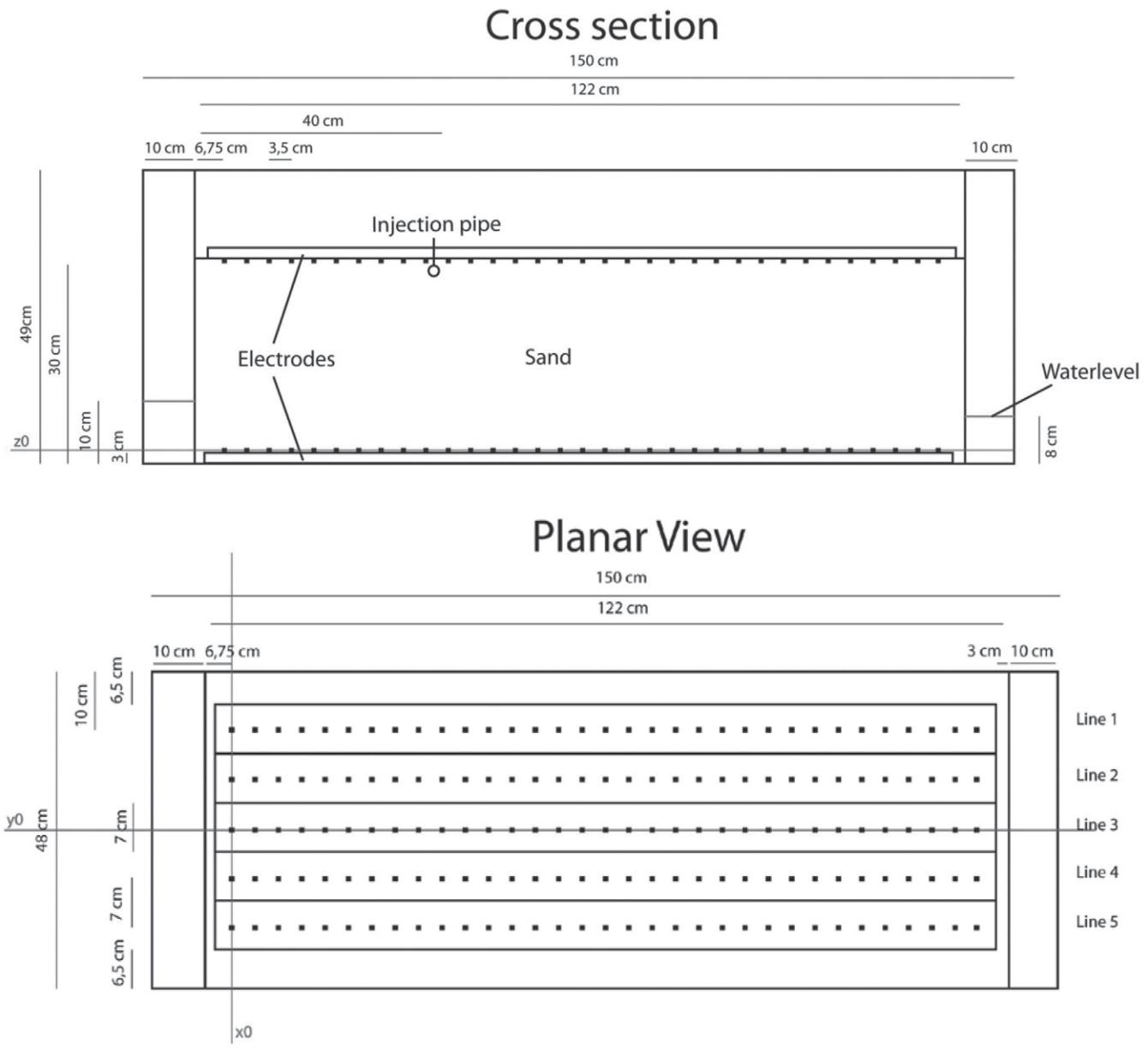

Fig. 1. The experimental setup.

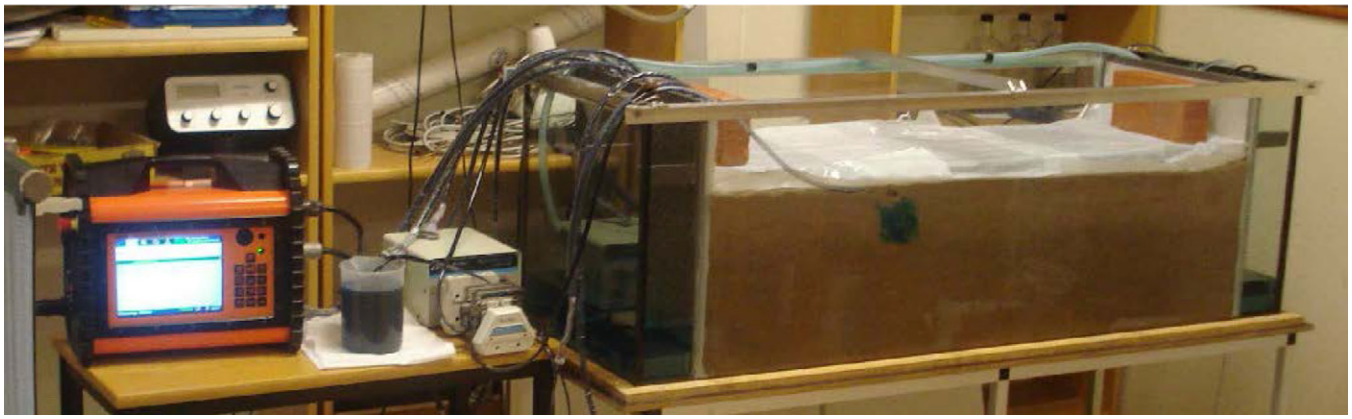

Fig. 2. The experimental setup during an ongoing injection experiment.

Solute Transport Experiments

Five experiments were conducted in the tank. Each experiment was started by adjusting the flow of the return pump circulating water from the right to left reservoir. The resulting water level in the left reservoir for each experiment is presented in Table 1. The tank was left for several hours to achieve steady-state conditions, then, at time $t = 0$, dye-stained water was applied through the application system. The injected dye was mixed with tap water (electrical conductivity around 0.3 S m^{-1}, pH = 8.3) and had a concentration of 4 g L^{-1} and an electrical conductivity of 0.097 to 0.105 S m^{-1}. Each experiment lasted between 4 and 7 h after starting the dye application. Between experiments, the water level in both reservoirs and the tank was raised to the soil surface and clean tap water was circulated through the tank to remove the dye tracer.

Optical Image Analysis

During the experiments, photographs were taken with a Nikon d2X digital camera using a 50-mm lens. The camera was placed 3 m in front of the tank. The time interval between the pictures was 30 min. The pictures were converted into a black and white image in Adobe Photoshop CS6 (Adobe Systems Inc.) using the thresholding method. The stained and unstained sand clearly produced two distinct maxima of the image histogram; the threshold was selected as the local minimum between these two maxima.

Table 1. Water level in the left reservoir, return flow (from the right to left reservoir), and dye application rate for the five experiments. Note that the water level in the right reservoir was kept constant at 0.08 m throughout all experiments.

Exp.	Left reservoir level	Return flow	Dye application rate
	m	L h^{-1}	
1	0.10	3.6	2
2	0.12	8	2
3	0.09	1.7	2
4	0.10	3.3	0.8
5	0.12	8	0.8

The horizontal velocity of the dye pulse in the CF was calculated by measuring the change in the location of the dye front between images. The calculations were made after the dye front passed about 0.6 m from the left side of the tank; at this distance the dye transport took place entirely in the CF in all experiments.

Resistivity Measurements

Electrical resistivity tomography has become a valuable tool for imaging solute transport and quantifying moisture content at various scales. At the laboratory scale, Binley et al. (1996) and Garré et al. (2010) used undisturbed soil columns, while Bechtold et al. (2012) used a soil of controlled grain-size distribution with well-known retention parameters to monitor and simulate vertical transport velocities for preferential upward flow pathways under evaporation conditions. Generally, the methods can be transferred to the field scale (e.g., Kemna et al., 2002) to study the saturated zone or the unsaturated zone (e.g., Beff et al., 2013).

A customized resistivity measurement system was created for the glass tank. Ten lines of electrodes, five in the bottom and five on top of the sand layer, contained a total of 320 electrodes. Each line consisted of a 1.17-m-long plastic board with 32 electrodes. The electrodes were 3 mm long, gold plated, and placed at a distance of 35 mm along the boards. A Wettex fabric (Vileda) layer was placed below the top electrodes to improve the galvanic contacts with the relative dry sand layer close to the surface. The data acquisition system allowed measurement of two lines at a time. Each electrode in the bottom was therefore measured at the same time as the corresponding electrode on top of the sand. These combinations of two electrodes are referred to as Lines 1 to 5 (Fig. 1). The five lines were measured cyclically throughout the whole experiment, starting with Line 1. Each measurement took approximately 10 to 12 min, which led to a time step of 60 min between two investigations.

An ABEM Terrameter LS was used to conduct the resistivity measurements. It is controlled via integrated firmware, with a graphical user interface that automatically carries out the measurements (e.g., Dahlin, 2001) according to predefined electrode

spread descriptions and measurement sequences. The instrument was connected directly to two lines of electrodes at a time as outlined above, and a combination of multiple-gradient array and cross-hole dipole–dipole array (Danielsen and Dahlin, 2010) was used for taking measurements along and between the electrodes on top of and in the bottom of the sand. A transmitted current of 2 mA and maximum output potential of around 250 V was used as the output signal for the measurements.

The collected data were exported to data formats suitable for data quality checking, processing, and inversion (inverse numerical modeling). BERT (Boundless Electrical Resistivity Tomography) was used for inversion to create three-dimensional hexahedral models of the investigated volume based on the measured resistances. Günther et al. (2006) described the inversion methodology used in detail; more descriptions from a hydrologic perspective were given by Bechtold et al. (2012) and Beff et al. (2013). Briefly, the norm of an error-weighted data misfit is minimized. We used L1 norm (robust) inversion due to inaccuracies occurring directly at the tracer injection. For estimating errors, Koestel et al. (2008) suggested a method of analyzing reciprocal data. Initial reciprocal tests before the injection showed values in the range of 1% that increased during the course of the experiment. Therefore, we chose a noise model of 3% plus a voltage error of 100 μV.

In addition to the data misfit, the roughness of the model is minimized. The regularization parameter that weights this term is determined such that the data are fitted within noise, i.e., the smoothest of all equivalent models that fit the data is chosen. There have been numerous studies that discussed the resolution limitations of ERT in the hydrologic framework (e.g., Day-Lewis et al., 2005; Koestel et al., 2009). The smoothness of the results depends on the experimental design, i.e., electrode positions and arrays, and the data errors. The bad coupling of the uppermost electrodes and the strongly heterogeneous resistivity contrast at the injection pipe significantly influenced data quality. Furthermore, it led to a strong contrast at the top layer that was temporally varying. Therefore we did not, as is very common, use a difference inversion scheme but inverted each data set independently.

The dimensions and boundary conditions of the experiment tank were incorporated in the three-dimensional models, and a different regularization strength was adjusted to optimize the data fit and thus model quality. Bechtold et al. (2012) described how inversion of the subsequent data sets was done for a similar rectangular model geometry. ParaView was used to visualize the inverted models in three dimensions. For imaging solute transport, we used the relative differences between the resistivity values taken during each time step of the experiments and the initial measurement that was taken before each experiment. As a consequence of smoothness constraints, the images showed diffuse boundaries that made a velocity computation difficult. A simple method is to use threshold values for the ratio; in this case values between 0.5 and 0.9 were tested. The location of the front was defined as the rightmost point with resistivity below this threshold. Values of the location of the front of all time steps were determined and a regression line was fit for estimating the velocity.

Hydraulic Modeling

The two-dimensional hydraulic model HYDRUS-2D (PC-Progress) was used to simulate water and solute transport in the tank. This software simulates two-dimensional movement of water, heat, and multiple solutes in variably saturated media based on finite-element numerical solutions of the flow equations (Šimůnek et al., 1999).

The simulated domain was 1.22 m wide and 0.3 m deep. An unstructured triangular mesh with 3018 elements (with a typical side length of 0.02 m) was used to spatially discretize the flow domain. The constant water level in the right and left water reservoirs was simulated using a constant-head boundary condition; all other boundaries were set to no flux except for the injection point.

The longitudinal dispersivity (ε_L) is a parameter that is difficult to estimate. Attempts have been made to relate ε_L to soil particle size or water retention characteristics (e.g., Perfect et al., 2002), but in many studies ε_L is calculated from tracer experiments using inverse modeling. We used several different values of ε_L in the range of 0.1 to 10 cm. The transversal dispersivity e_T is normally smaller than the longitudinal one; ratios of ε_L/e_T between 1 and 100 have been reported in the literature (e.g., Bear and Verruijt, 1987; Delgado, 2007). In the present study, we chose to set $e_T = 0.1\varepsilon_L$, a ratio that has been used successfully in several HYDRUS applications (e.g., Pang et al., 2000; Hanson et al., 2006; Selim et al., 2013). The molecular diffusion was set to 0 because it was assumed to be negligible for the rather high solute transport velocities used in this study. The linearized Freundlich isotherm coefficient, K_d, of the dye used has been shown to depend on clay content and pH (e.g., Germán-Heins and Flury, 2000). In the present study, K_d was set equal to 100 $cm^3\ kg^{-1}$; similar values have previously been reported for sandy soils by, e.g., Flury and Flühler (1995) and Öhrström et al. (2004).

The hydraulic parameters of the sand were estimated by filling a 0.75-m-high Plexiglas tube with sand. The bottom of the column was in contact with a water reservoir. The sand was saturated and then left to drain for 24 h. The water content distribution was estimated by image analysis (Persson, 2005a), and the best fitting hydraulic parameters of the van Genuchten model (van Genuchten, 1980) were optimized (residual water content = 0.045 $m^3\ m^{-3}$, saturated water content = 0.43 $m^3\ m^{-3}$, $\alpha = 0.07\ cm^{-1}$, $n = 8.4$). The saturated hydraulic conductivity (K_{sat}) was calculated using Darcy's law using the measured return flow for each gradient. The average K_{sat} calculated during the five experiments was 122 m d^{-1} with a standard deviation of 9.1 m d^{-1}.

First, the simulation was run for 24 h without adding any solutes. Then a pulse of the Brilliant Blue solution was applied to the

injection point for 7 h. To facilitate comparison with the optical dye images, the simulated concentration was converted to black and white images using the threshold 0.1 g L^{-1}, which is the lower limit of visual detection of the dye in light-colored soils (e.g., Ewing and Horton, 1999; Öhrström et al., 2004). The horizontal velocity of the dye plume front was calculated in the same way as the one measured from the dye images.

Results and Discussion

Optical Image Analysis

Black and white images of the dye transport with a 30-min time increment in the five experiments are presented in Fig. 3. The horizontal movement in the CF was strong in all experiments; the dye did not enter the saturated zone until it reached the right end of the tank. The measured horizontal velocities of the dye plume fronts are presented in Table 2. At the same dye application rate, the horizontal velocity was strongly dependent on the gradient—a higher gradient gave a higher horizontal velocity. When comparing experiments with the same gradient, it was evident that a higher dye application rate led to higher horizontal velocity. The vertical penetration of the dye in the CF was also dependent on both the gradient and the dye application rate. At higher gradients, the penetration of the dye in the CF was restricted; for low gradients, the dye penetrated the entire CF. Furthermore, a higher dye application rate resulted in a deeper penetration.

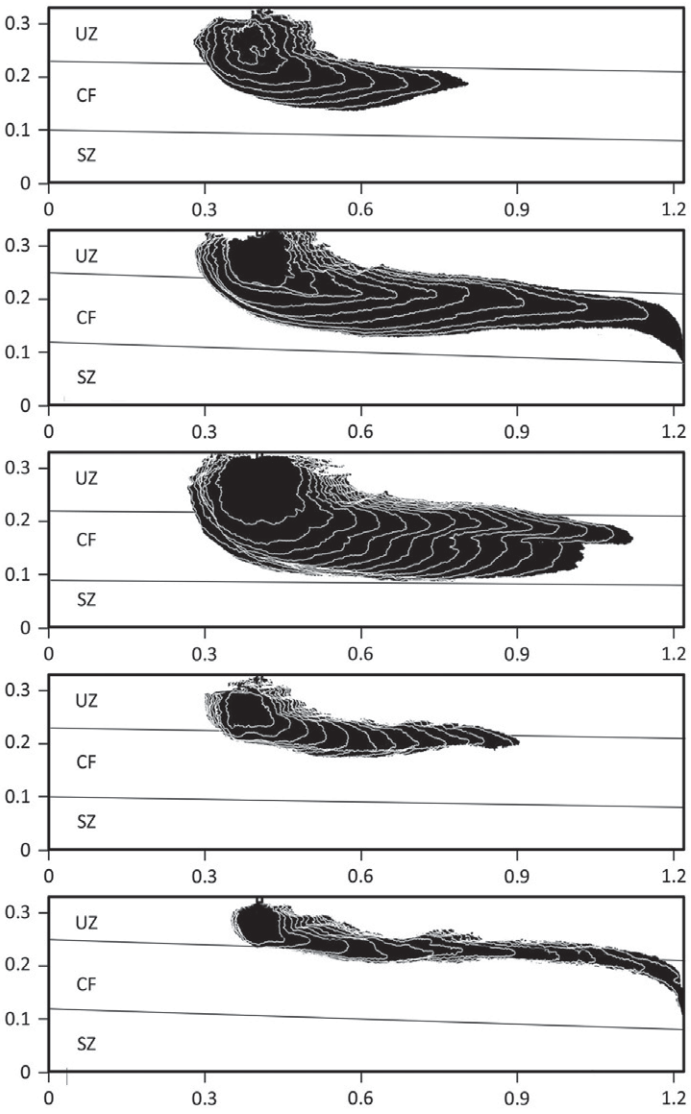

Fig. 3. Dye distribution determined by optical image analysis during Exp. 1 (top) to 5 (bottom). The solid lines show the approximate extent of the unsaturated zone (UZ), capillary fringe (CF), and saturated zone (SZ). Horizontal and vertical scales are in meters.

Electrical Resistivity Tomography

The resistivity monitoring resulted in distinct changes in measured apparent resistivities for all experiments, and the tracer plume was clearly visible in the inverted resistivity models as exemplified in Fig. 4. In the resistivity models, there was a very distinct change in resistivity at the upper limit of the CF, with an elevation of the resistivity gradient below the tracer injection line. In some of the experiments the resistivity models showed clear evidence of uneven injection of the tracer, for example Exp. 2 (Fig. 4a), and partial surficial lateral spreading of the tracer, which is in accordance with observations made during the experiments. This led to modification of the injection mechanism, which improved the performance in the following experiments.

The change in resistivity as a result of the tracer became clearer when plotted as a difference or ratio relative to the background measurement taken before injection started. As can be seen in the example results of Exp. 2 (Fig. 5) and Exp. 4 (Fig. 6), the developing decrease in resistivity had the visual appearance of tracer plumes. These plumes largely followed the same patterns as the optical image analysis (Fig. 3), with strong horizontal movement. One significant difference is that the resistivity plumes have rather diffuse transitions to the unaffected surrounding volumes compared with the optical images. It should be noted that since the background measurement was taken before the start of the water injection at

Table 2. Horizontal velocity at 0.6-m vertical distance assuming the same velocity in both the saturated zone (SZ) and the capillary fringe (CF), velocity of the dye plume front in the CF measured using optical image analysis and electrical resistivity tomography (ERT), and velocity of the dye plume front in the CF simulated using HYDRUS-2D. For resistivity, three different threshold values were used for the ratio.

Exp.	Velocity in SZ + CF	Optical image analysis	ERT			HYDRUS-2D
			0.6	0.7	0.8	
			cm h^{-1}			
1	12	12	17.0	16.0	16.0	14
2	21	22	25.4	24.0	22.6	25
3	8	10	11.0	11.8	12.0	9
4	9	10	9.8	11.2	10.2	9
5	19	17	15.2	16.8	15.6	17

the sand surface, the increase in water content directly below the injection point resulted in an additional decrease in the resistivity. Therefore, the resistivity measurement in the unsaturated zone should be considered uncertain. The resistivity plumes are wider both laterally and vertically than the optical images, where more horizontal spreading in the upstream direction is evident. They also follow a deeper path, which however always stays above the saturated zone. A few odd anomalous spots at the surface in the models change positions in an arbitrary way, which is indicative of some noise in the data, but apart from that the resistivity models have a very consistent appearance.

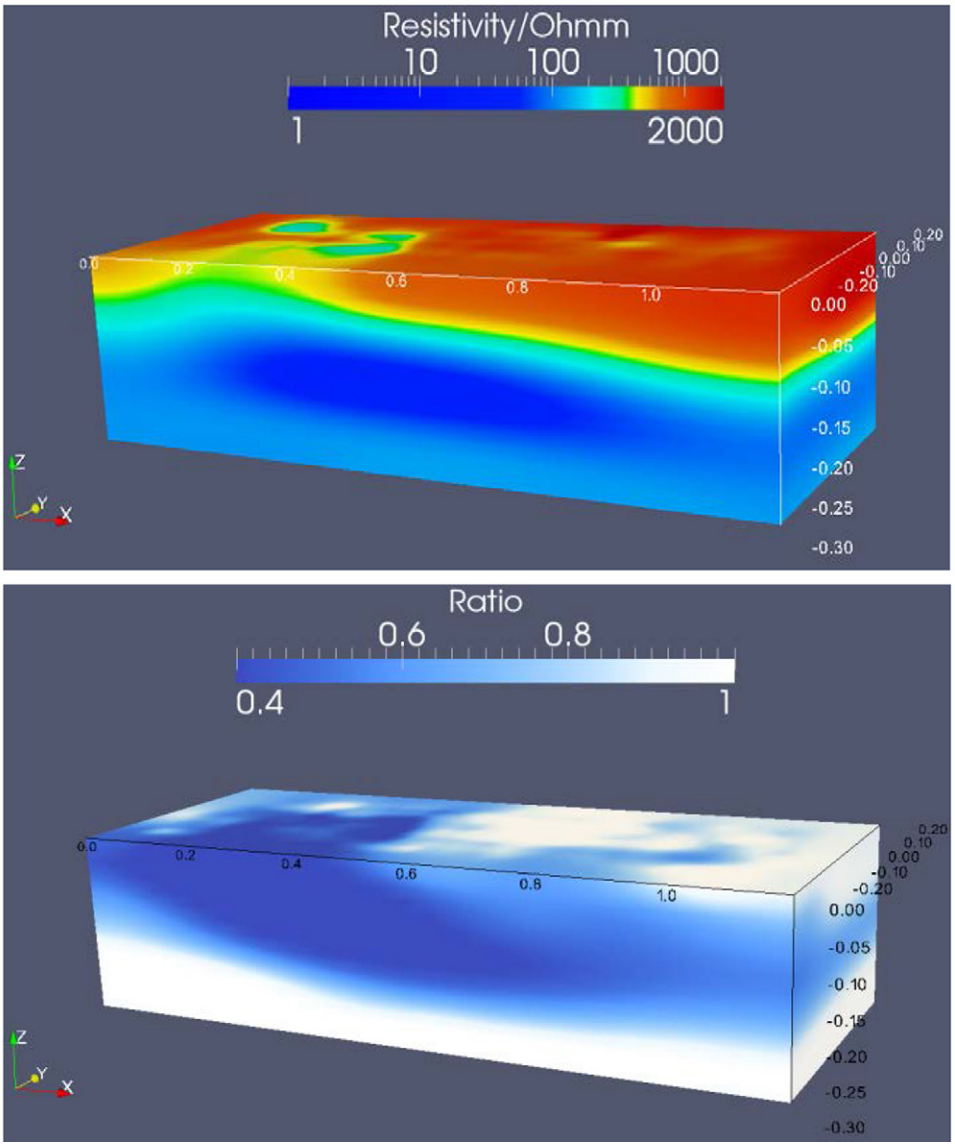

Fig. 4. Examples of (a) inverted three-dimensional resistivity models after completion of Exp. 2, and (b) resistivity change (ratio) from the initial model.

The more gradual transitions of the resistivity models might be explained in different ways. One explanation is that there is a threshold limit in the dye concentration when it becomes visible. When the concentration is lower than this limit, no dye can be visually observed; however, it can still lower the resistivity. Another factor to bear in mind is that the smooth inversion technique generally creates models with smooth transitions, but since L1 norm (blocky) inversion was used, this should be less pronounced than if L2 norm (smooth) inversion had been used. Furthermore, equivalence, i.e., that a number of different models can explain the data within the error range, may also play a role in the inversions and could lead to exaggerated vertical extension of the plumes. This is particularly true because bad electrode coupling leads to higher errors and thus smoother models. A main factor, however, is that one measuring cycle (50 min) can hardly be assumed to be associated with a constant resistivity model. Hence, temporal smearing adds to the smoothness of the inversion routine. Rigorously excluding temporal smoothing would require immense modifications of the data analysis. So far, no robust algorithm is available and developing one was beyond the scope of this study. A simple procedure is to interpolate the data onto common time points. Tests showed that this did not significantly improve the images, which however cannot be interpreted as an absence of temporal smoothing but as a shortcoming of the method. For the presented case, there are some effects limiting the ERT image quality (smoothness), but because the data are gathered in slices, the effect is not too severe and will hardly affect the velocity analysis.

The horizontal velocities measured using ERT for three different ratios are presented in Table 2. As can be seen, the horizontal velocities were not highly affected by the different threshold ratios, but the ratio 0.7 seemed to fit the values measured by the optical image analysis best.

Hydraulic Modeling

The value of ε_L that gave the best visual agreement between the numerical hydraulic model and the observed dye distribution was 1 cm; therefore this value was used in all modeling presented below. Even when ε_L was set to 0.1 or 10 cm, the horizontal velocity of the simulated dye plume was still within around 10% of the value obtained using ε_L = 1 cm (data not shown). We also checked the model sensitivity for K_{sat} by using the values of 112.9 and 131.1 m d^{-1}; these values correspond to the average of the

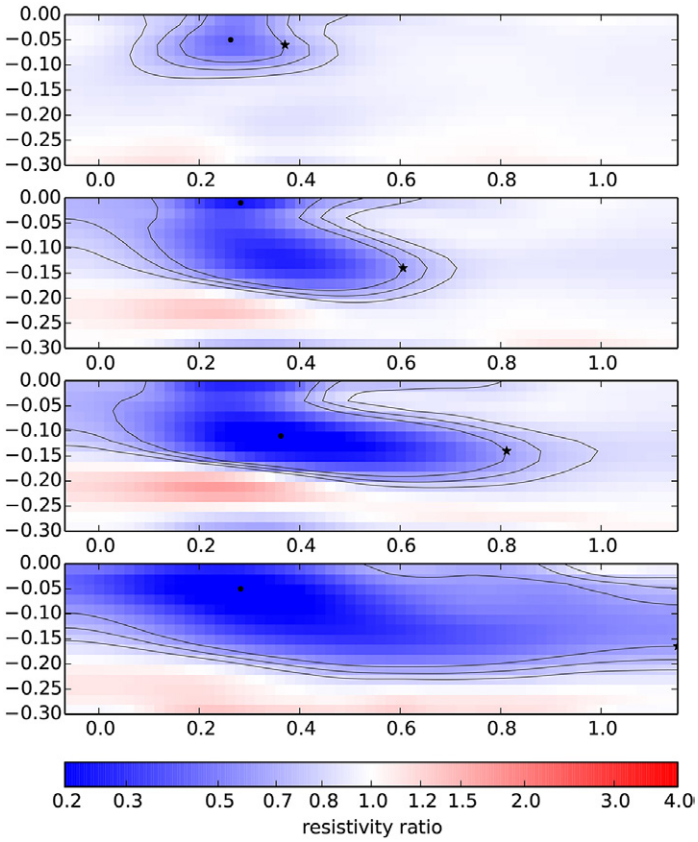

Fig. 5. Ratio of resistivity after (a) 1 h, (b) 2 h, (c) 3 h, and (d) 4 h relative to background measurement before tracer injection started for Exp. 2. Contour lines refer to values of 0.6, 0.7, and 0.8, the point is the maximum change, and the star denotes the rightmost position of the 0.8 contour line.

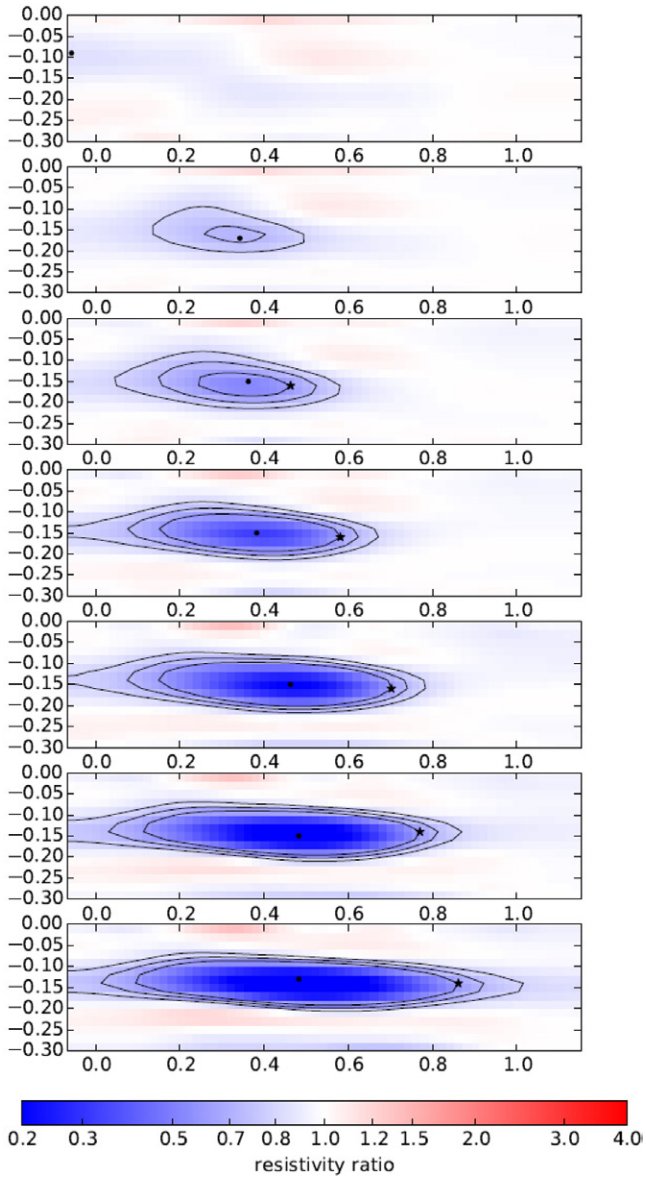

Fig. 6. Ratio of resistivity after 1, 2, 3, 4, 5, 6, and 7 h (from top to bottom) relative to background measurement before tracer injection started for Exp. 4. Contour lines refer to values of 0.6, 0.7, and 0.8, the point is the maximum change, and the star denotes the rightmost position of the 0.8 contour line.

estimated K_{sat} plus and minus the standard deviation. This led to a change in the horizontal velocity of <10%.

In Fig. 7, the results of the numerical simulation are presented. The figure shows the simulated dye distribution 2, 3, and 4 h after the start of the dye application for each experiment. The general patterns are similar to the measured results using optical image analysis and resistivity. The horizontal velocities measured from the numerical simulations are presented in Table 2.

Comparison between Measured and Simulated Horizontal Velocities

The dye distribution observed by optical image analysis presented in Fig. 3 was observed through the front glass of the experimental tank. It should be noted that the dye distribution could be different inside the sand volume. During the experiments, we also manually inspected the dye distribution on the back side of the tank. The dye distribution was similar, but especially in Exp. 1 and 2 the dye plumes reached longer along the back side. When inspecting the dye application system, we found that the hole closest to the front glass was partially clogged. In subsequent experiments, we made sure that the dye could flow freely through this hole. This explains why the dye distribution for the first hour is different in Exp. 1 to 3 even though the dye application rate was the same. This is also the reason why we chose to measure the horizontal velocity of the dye plume after it passed 0.6 m; at this distance we believe that the effects of a slower dye application rate close to the front glass was negligible. When the optical image analysis dye distribution is compared with the hydraulic model results, it is also evident that the dye plume advancement was slower during the first hour with the exception of Exp. 3.

The resistivity models show that the intention to distribute the tracer evenly along a pipe perpendicular to the groundwater flow direction was not entirely successful, at least not in the first two experiments. We believe, however, that this had a limited effect on the measured values of the horizontal velocity.

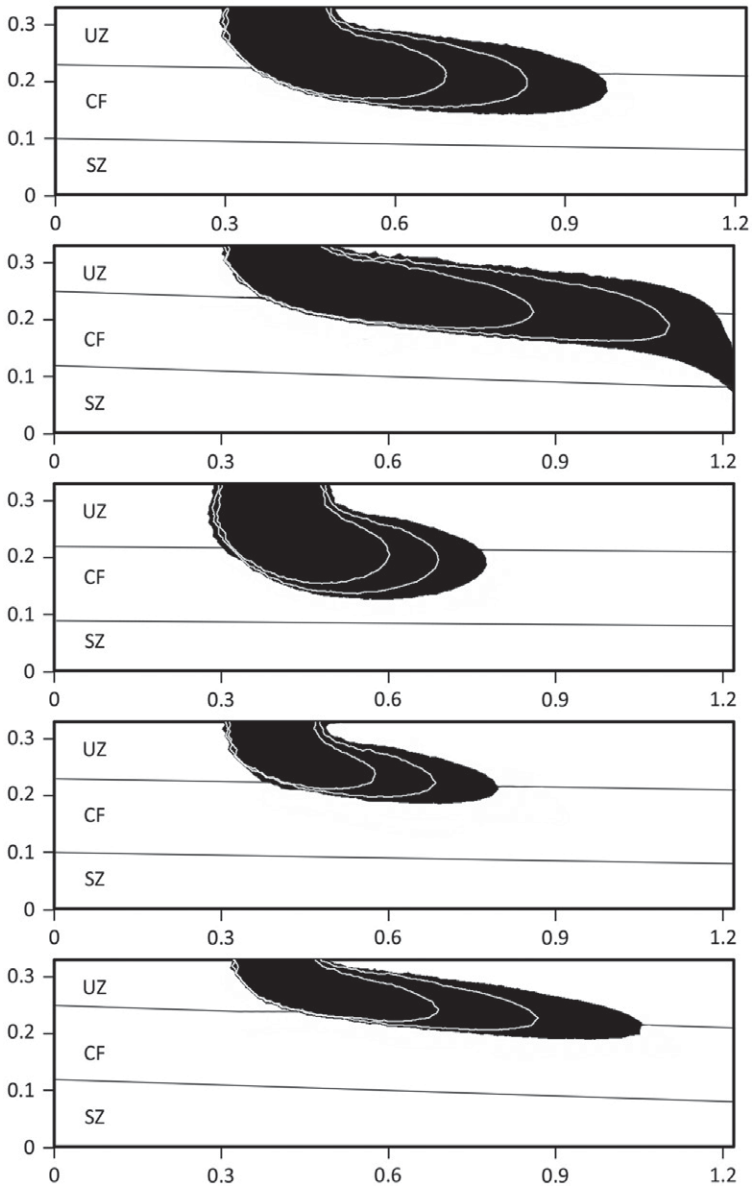

Fig. 7. HYDRUS-2D simulations of dye distribution 2, 3, and 4 h after the start of dye application in Exp. 1 (top) to 5 (bottom). The solid lines show the approximate extent of the unsaturated zone (UZ), capillary fringe (CF), and saturated zone (SZ). Horizontal and vertical scales in meters.

The simulated horizontal velocities were, in general, very close to the ones measured. Differences are probably related to uncertainties in the estimated hydraulic parameters of the sand, especially the hydraulic conductivity. Although care was taken to pack the sand as uniformly as possible, it is also probable that heterogeneity affected the results somewhat. Still, the similarity between the measured and simulated dye distributions is encouraging.

Horizontal Velocities in the Capillary Fringe and Saturated Zone

In both the experimental results and the numerical simulation, we saw a strong horizontal movement of the dye in the CF. If we assume that the horizontal velocity of the saturated zone and the CF is the same, the velocity v at the middle of the tank along the long axis can be calculated by

$$v = \frac{Q_{tot}}{\theta A_{CF+SZ}} \quad [1]$$

where Q_{tot} is the sum of the return flow and the dye application rate, θ is the water content (0.43 m^3 m^{-3} because both the saturated zone and the CF is assumed to be fully saturated), and A_{CF+SZ} is the cross-sectional area of the saturated zone and the CF, calculated by

$$A_{CF+SZ} = \left(\frac{WL_R + WL_L}{2} + H_{CF} \right) D \quad [2]$$

where WL_R and WL_L are the water levels in the right and left reservoirs, respectively, H_{CF} is the height of the CF (0.13 m in all experiments), and D is the width of the tank. The resulting v for each experiment is presented in Table 2. The calculated values of v are almost identical to the measured velocities using optical image analysis. The values calculated from the resistivity measurements were determined using three different ratio thresholds. All three thresholds are comparable and agree well with the values measured using the other two methods but tended to overestimate the velocity values slightly.

In the hydraulic model, the soil water velocity vectors could be studied. This showed that the velocity was identical in both the saturated zone and the lower part of the CF. In the upper part of the CF, the velocity rapidly decreased. The hydraulic gradient is still the same, but as the height above the groundwater table increases, both water content and hydraulic conductivity will decrease, leading to a lower velocity. The hydraulic parameters of the soil will determine at what height the velocity will start to decrease and how steep the decrease is.

The results presented here are consistent with the findings of Berg and Gillham (2010), who measured the horizontal water velocity using a point velocity probe in a laboratory experiment. They showed that the water velocity profile was continuous from below the water table up to 0.44 m above the water table, corresponding to the air-entry pressure of the sand used. Above this level, the velocity decreased sharply.

Summary and Conclusion

Five solute transport experiments were conducted in the laboratory to study transport in the capillary fringe. The solute transport was measured using both optical image analysis and resistivity measurements. The results showed that the solutes were transported horizontally in the CF, not entering the saturated zone until the

end of the experimental tank. The horizontal velocity was identical in the saturated zone and the CF. This can have very important practical implications for contaminant sampling strategies; if contaminants are also transported across significant distances in the CF at the field scale, sampling only in the saturated zone may miss the contaminants.

The resistivity results clearly delineate tracer plumes that are, for all the experiments, in general agreement with the optical image analysis. The resistivity plumes generally have a larger vertical and horizontal extension than the optical images. This might be a result of the inversion process. It is also possible that the tracer distribution is different inside the sand volume than at the glass wall, which is the only part of the volume that could be observed visually. Finally, it is likely that the visual detection limit is different from the detection limit for differential resistivity analysis.

Although there is not a perfect match between the resistivity images and the optical image analysis, it is evident that the shape and progress of the tracer plume was captured by the resistivity monitoring. This is important because the technique can be applied in the field where visual observation of the tracer is not an option. In environmental protection applications, the technique could be used to image and monitor the subsurface in three dimensions for contaminant plume delineation, which could be used as a basis for designing an optimized drilling and sampling program. This can be critical in actual geological environments where contaminants may follow preferential flow paths and be missed if drilling and sampling is done in arbitrary positions.

If an appropriate threshold for the resistivity change is used (in our case 0.7), tracer plume velocity can be estimated from the ERT results in good accordance with the values from the optical image analysis. However, the parameters of both inversion and velocity determination must be well chosen or calibrated in the field. This becomes more difficult if field layouts of limited coverage and data quality are used or if fingering plays a non-negligible role. In field applications where no optical images are available, the threshold ratio of the resistivity can be chosen on the basis of synthetic models, in situ measurements of electrical conductivity, or sample analyses results. Synthetic models might also be used for guidance.

Our results show that from a water transport perspective, the CF acts in the same way as the saturated zone; the gradient, water content, and hydraulic conductivity, and thus both the magnitude and direction of the velocity, are the same. This is true up to a level above the groundwater surface where both the water content and hydraulic conductivity do not significantly deviate from the saturated values. Where this level is situated exactly depends on the hydraulic characteristics. A proper definition of the upper boundary of the CF, from a water transport perspective, must include constraints for both the water content and hydraulic conductivity decrease. Further studies in several different soil types are needed for quantification. Apart from ERT, other geophysical methods such as magnetic resonance may be used to characterize the van Genuchten parameters of the soil (Costabel and Günther, 2014) or the dynamics of soil moisture in the field.

The experimental results obtained in the present study were well described by the hydraulic model HYDRUS-2D. This shows that the model can be used for further transport studies in the CF, at least in homogeneous soils. A fluctuating groundwater table, air entrapment, and soil heterogeneities can probably significantly affect the horizontal velocity. Further studies, both in the laboratory and the field, as well as numerical studies are necessary.

Acknowledgments

This study was funded by the Geological Survey of Sweden (SGU) through the grant "Water and solute transport processes across the capillary fringe" (60-1658/2009). Pontus Pojmark and Benedict Rumpf conducted most of the laboratory experiment; their help is greatly acknowledged. Kristofer Hellman made important contributions to the inversion of the resistivity data.

References

Abdul, A.S., and R.W. Gillham. 1984. Laboratory studies of the effects of the capillary fringe on streamflow generation. Water Resour. Res. 20:691–698. doi:10.1029/WR020i006p00691

Abit, M.A., Jr., A. Amoozegar, M.J. Vepraskas, and C.P. Niewoehner. 2012. Soil and hydrologic effects on fate and horizontal transport in the capillary fringe of surface-applied nitrate. Geoderma 189–190:343–350. doi:10.1016/j.geoderma.2012.05.029

Bear, J. 1972. Dynamics of fluids in porous media. Elsevier, New York.

Bear, J., and A. Verruijt. 1987. Modelling groundwater flow and pollution. D. Reidel Publ. Co., Dordrecht, the Netherlands.

Bechtold, M., J. Vanderborght, L. Weihermüller, M. Herbst, T. Günther, O. Ippisch, et al. 2012. Upward transport in a three-dimensional heterogeneous laboratory soil under evaporation conditions. Vadose Zone J. 11(2). doi:10.2136/vzj2011.0066

Beff, L., T. Günther, B. Vandoorne, V. Couvreur and M. Javaux. 2013. Three-dimensional monitoring of soil water content in a maize field using electrical resistivity tomography. Hydrol. Earth Syst. Sci. 17:595–609. doi:10.5194/hess-17-595-2013

Berg, S.J., and R.W. Gillham. 2010. Studies of water velocity in the capillary fringe: The point velocity probe. Ground Water 48:59–67. doi:10.1111/j.1745-6584.2009.00606.x

Berkowitz, B., S.E. Silliman, and A.M. Dunn. 2004. Impact of the capillary fringe on local flow, chemical migration, and microbiology. Vadose Zone J. 3:534–548. doi:10.2136/vzj2004.0534

Binley, A., S. Henry-Poulter, and B. Shaw. 1996. Examination of solute transport in an undisturbed soil column using electrical resistance tomography. Water Resour. Res. 32:763–769. doi:10.1029/95WR02995

Cho, H., and G.H. de Rooij. 2002. Pressure head distribution during unstable flow in relation to the formation and dissipation of fingers. Hydrol. Earth Syst. Sci. 6:763–771. doi:10.5194/hess-6-763-2002

Costabel, S., and T. Günther. 2014. Noninvasive estimation of water retention parameters by observing the capillary fringe with magnetic resonance sounding. Vadose Zone J. 13(6). doi:10.2136/vzj2013.09.0163

Dahlin, T. 2001. The development of electrical imaging techniques. Comput. Geosci. 27:1019–1029. doi:10.1016/S0098-3004(00)00160-6

Danielsen, B.E., and T. Dahlin. 2010. Numerical modelling of resolution and sensitivity of ERT in horizontal boreholes. J. Appl. Geophys. 70:245–254. doi:10.1016/j.jappgeo.2010.01.005

Day-Lewis, F.D., K. Singha, and A.M. Binley. 2005. Applying petrophysical models to radar travel time and electrical resistivity tomograms: Resolution-dependent limitations. J. Geophys. Res. 110:B08206. doi:10.1029/2004JB003569

Delgado, J.M.P.Q. 2007. Longitudinal and transverse dispersion in porous media. Chem. Eng. Res. Des. 85:1245–1252. doi:10.1205/cherd07017

Dunn, A.M., S.E. Silliman, S. Dhamwichukorn, and C.F. Kulpa. 2005. Demonstration of microbial transport into the capillary fringe

via advection from below the water table. J. Hydrol. 306:50–58. doi:10.1016/j.jhydrol.2004.08.035

Ewing, R.P., and R. Horton. 1999. Discriminating dyes in soil with color image analysis. Soil Sci. Soc. Am. J. 63:18–24. doi:10.2136/sssaj1999.03615995006300010004x

Flury, M., and H. Flühler. 1994. Brilliant Blue FCF as a dye tracer for solute transport studies: A toxicological overview. J. Environ. Qual. 23:1108–1112. doi:10.2134/jeq1994.00472425002300050037x

Flury, M., and H. Flühler. 1995. Tracer characteristics of Brilliant Blue FCF. Soil Sci. Soc. Am. J. 59:22–27. doi:10.2136/sssaj1995.03615995005900010003x

Freitas, J.G., and J.F. Barker. 2011. Monitoring lateral transport of ethanol and dissolved gasoline compounds in the capillary fringe. Ground Water Monit. Rem. 31:95–102. doi:10.1111/j.1745-6592.2011.01338.x

Freitas, J.G., and J.F. Barker. 2013. Denatured ethanol release into gasoline residuals:1. Source behavior. J. Contam. Hydrol. 148:67–78. doi:10.1016/j.jconhyd.2012.12.010

Garré, S., J. Koestel, T. Günther, M. Javaux, J. Vanderborght, and H. Vereeken. 2010. Comparison of heterogeneous transport processes observed with electrical resistivity tomography in two different soils. Vadose Zone J. 9:336–349. doi:10.2136/vzj2009.0086

Germán-Heins, J., and M. Flury. 2000. Sorption of Brilliant Blue FCF in soils as affected by pH and ionic strength. Geoderma 97:87–101. doi:10.1016/S0016-7061(00)00027-6

Gillham, R.W. 1984. The capillary fringe and its effect on water-table response. J. Hydrol. 67:307–324. doi:10.1016/0022-1694(84)90248-8

Günther, T., C. Rücker, and K. Spitzer. 2006. Three-dimensional modelling and inversion of DC resistivity data incorporating topography: II. Inversion. Geophys. J. Int. 166:506–517. doi:10.1111/j.1365-246X.2006.03011.x

Hanson, B.R., J. Šimůnek, and J.W. Hopmans. 2006. Evaluation of urea–ammonium-nitrate fertigation with drip irrigation using numerical modeling. Agric. Water Manage. 86:102–113. doi:10.1016/j.agwat.2006.06.013

Henry, E.J., and J.E. Smith. 2002. The effect of surface-active solutes on water flow and contaminant transport in variably saturated porous media with capillary fringe effects. J. Contam. Hydrol. 56:247–270. doi:10.1016/S0169-7722(01)00206-6

Kemna, A., J. Vanderborght, B. Kulessa, and H. Vereecken. 2002. Imaging and characterisation of subsurface solute transport using electrical resistivity tomography (ERT) and equivalent transport models. J. Hydrol. 267:125–146. doi:10.1016/S0022-1694(02)00145-2

Klenk, I.D., and P. Grathwohl. 2002. Transverse vertical dispersion in groundwater and the capillary fringe. J. Contam. Hydrol. 58:111–128. doi:10.1016/S0169-7722(02)00011-6

Koestel, J.K., R. Kasteel, A. Kemna, O. Esser, M. Javaux, A. Binley, and H. Vereecken. 2009. Imaging Brilliant Blue stained soil by means of electrical resistivity tomography. Vadose Zone J. 8:963–975. doi:10.2136/vzj2008.0180

Koestel, J.K., A. Kemna, M. Javaux, A. Binley, and H. Vereecken. 2008. Quantitative imaging of solute transport in an unsaturated and undisturbed soil monolith with 3-D ERT and TDR. Water Resour. Res. 44:W12411. doi:10.1029/2007WR006755

Lehmann, P., F. Stauffer, C. Hinz, O. Dury, and H. Flühler. 1998. Effect of hysteresis on water flow in a sand column with a fluctuating capillary fringe. J. Contam. Hydrol. 33:81–100. doi:10.1016/S0169-7722(98)00066-7

Öhrström, P., Y. Hamed, M. Persson, and R. Berndtsson. 2004. Characterizing unsaturated solute transport by simultaneous use of dye and bromide. J. Hydrol. 289:23–35. doi:10.1016/j.jhydrol.2003.10.014

Pang, L., M.E. Close, J.P.C. Watt, and K.W. Vincent. 2000. Simulation of picloram, atrazine, and simazine leaching through two New Zealand soils and into groundwater using HYDRUS-2D. J. Contam. Hydrol. 44:19–46. doi:10.1016/S0169-7722(00)00091-7

Perfect, E., M.C. Sukop, and G.R. Haszler. 2002. Prediction of dispersivity for undisturbed soil columns from water retention parameters. Soil Sci. Soc. Am. J. 66:696–701. doi:10.2136/sssaj2002.6960

Persson, M. 2005a. Estimating surface soil moisture from soil color using image analysis. Vadose Zone J. 4:1119–1122. doi:10.2136/vzj2005.0023

Persson, M. 2005b. Accurate dye tracer concentration estimations using image analysis. Soil Sci. Soc. Am. J. 69:967–975. doi:10.2136/sssaj2004.0186

Pojmark, P., B. Rumpf, T. Dahlin, M. Persson, and T. Günther. 2011. Resistivity imaging and image analysis for estimating water and solute transport across the capillary fringe in laboratory experiments. Vatten 67:193–198.

Ronen, D., H. Scher, and M. Blunt. 1997. On the structure and flow processes in the capillary fringe of phreatic aquifers. Transp. Porous Media 28:159–180.

Ronen, D., H. Scher, and M. Blunt. 2000. Field observations of a capillary fringe before and after a rainy season. J. Contam. Hydrol. 44:103–118. doi:10.1016/S0169-7722(00)00096-6

Selim, T., F. Bouksila, R. Berndtsson, and M. Persson. 2013. Soil water and salinity distribution under different treatments of drip irrigation. Soil Sci. Soc. Am. J. 77:1144–1156. doi:10.2136/sssaj2012.0304

Silliman, S., B. Berkowitz, J. Šimůnek, and M.Th. van Genuchten. 2002. Fluid flow and solute migration within the capillary fringe. Ground Water 40:76–84. doi:10.1111/j.1745-6584.2002.tb02493.x

Sinke, A.J.C., O. Dury, and J. Zobrist. 1998. Effects of a fluctuating water table: Column study on redox dynamics and fate of some organic pollutants. J. Contam. Hydrol. 33:231–246. doi:10.1016/S0169-7722(98)00072-2

Šimůnek, J., M. Šejna, and M.Th. van Genuchten. 1999. The Hydrus-2D software package for simulating the two-dimensional movement of water, heat, and multiple solutes in variably-saturated media. IGWMC-TPS 53, Version 2.0. Int. Ground Water Model. Ctr., Colorado School of Mines, Golden.

van Genuchten, M.Th. 1980. A closed-form equation for predicting the hydraulic conductivity of unsaturated soils. Soil Sci. Soc. Am. J. 44:892–898. doi:10.2136/sssaj1980.03615995004400050002x

Wyckoff, R.D., H.G. Botset, and M. Muskat. 1932. Flow of liquids through porous media under the action of gravity. J. Appl. Phys. 3:90–113.